Supplementary Material

The preparation of a fluorescent dual-modality nanosensor for the discrimination and determination of biothiols in real samples and its practical detection kit

İpek Ömeroğlu[a], Vildan Sanko[a, b, c], Ahmet Şenocak[a], Süreyya Oğuz Tümay[a,d]*

[a]Department of Chemistry, Gebze Technical University, Kocaeli 41400, Türkiye

[b]Department of Chemistry, Hacettepe University, Ankara 06800, Türkiye

[c] METU MEMS Center, Ankara, 06530, Turkey

[d]Department of Chemistry, Atatürk University, Erzurum 25240, Türkiye

*Corresponding author:

Dr. Süreyya Oğuz TÜMAY

e-mail: sotumay@atauni.edu.tr

1.1. Characterization of Nap-Br and 1

As can be seen in FTIR spectra, the vibrations observed at 3267 (-OH), 3057 (aromatic-CH), 2923-2852 (aliphatic-CH), 1603, 1509, and 1465 cm^{-1} (C-C) support the chemical structure of **Nap-Br** (Figure S1a). In addition, the $[M-C_8H_{16}Br]^+$ and $[M-CH_2Br]^+$ fractions were observed at 173.574 and 272.824 m/z whereas the $[M]^+$ molecular ion peak was observed at 365.079 m/z which were in good agreement with the structure (Figure S1b). The aromatic protons of **Nap-Br** were observed as 2H and 4H multiples between 7.55-7.48 ppm and 7.04-7.01 ppm, respectively. The -O-CH_2 and Br-CH_2 protons were obtained at 3.97 ppm (J: 6.55 Hz) and 3.34 ppm (J: 6.96 Hz), respectively, while other aliphatic protons were observed between 1.80-1.18 ppm which were compatible with the structure (Figure S1c). The aromatic and aliphatic carbon atoms were obtained at 154.50, 150.74, 128.68, 127.35, 126.99, 126.67, 118.16, 117.00, 108.65, 105.94, 67.02, 33.02, 31.78, 28.68, 28.47, 28.27, 27.68, 27.13, and 25.05 ppm, respectively (Figure S1d).

The FTIR and mass spectra of **1** were given in Figure S2a and b. As depicted, both the FTIR absorptions at 3059 (Aromatic-CH), 2920-2853 (aliphatic-CH), 1603, 1509, 1455 (C-C), 1538 (NO_2), 1375 cm^{-1} (NO_2) and the $[M]^+$ molecular ion peak which observed at 528.180 m/z supported proposed chemical structure of **1**. As can be seen from ^1H NMR (Figure S2c), the aromatic protons are observed as 8H multiples between 8.83-7.08 ppm while the peaks of -O-CH_2 and Br-CH_2 protons are obtained at 4.04 ppm and 3.54 ppm, respectively. The other aliphatic protons were observed as 14H multiples between 1.84-1.26 ppm. The aromatic and aliphatic carbon atoms were obtained at 157.93, 155.50, 145.88, 145.32, 145.24, 145.03, 144.27, 144.15, 143.98, 142.38, 142.21, 129.68, 129.16, 119.18, 106.97, 67.79, 32.62, 29.51, 29.36, 29.29, 29.13, 26.09 ppm. The chemical shifts, splitting and integrals of peaks in NMR spectra are compatible with the structure of **1**.

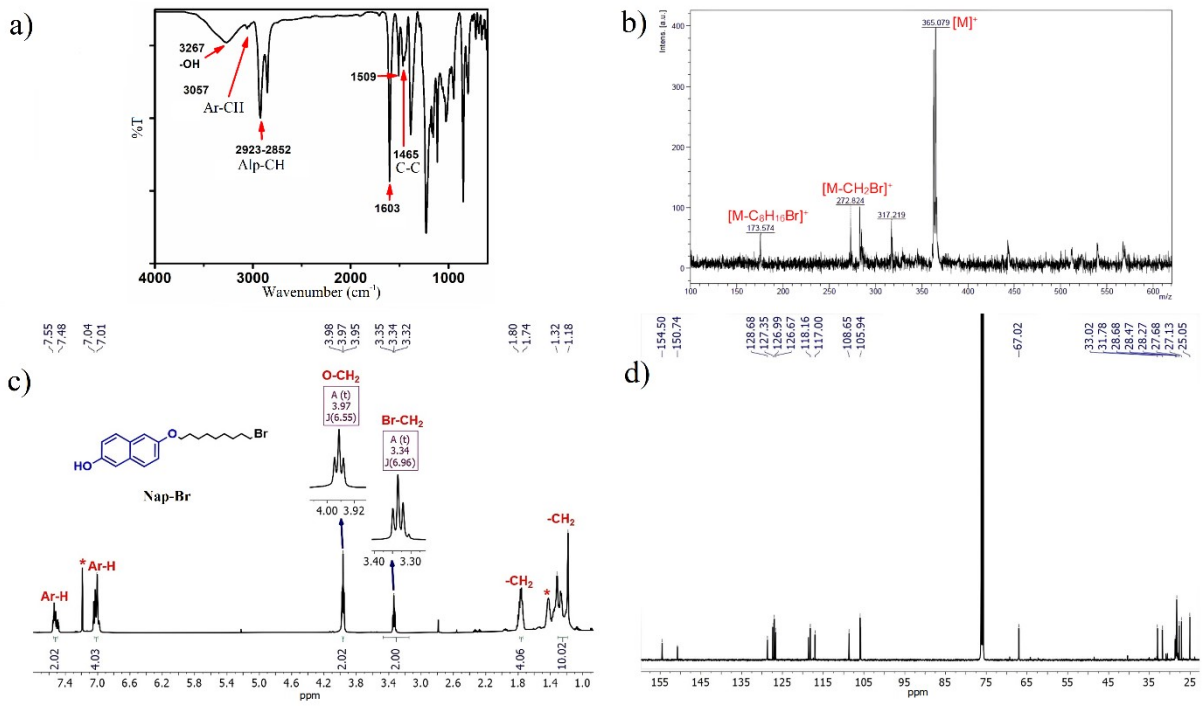

Figure S1. The structural characterization of of Nap-Br; **a)** FTIR, **b)** mass, **c)** ^{1}H NMR, and **d)** ^{13}C NMR spectra of Nap-Br. ($CDCl_3$ was used for NMR spectra).

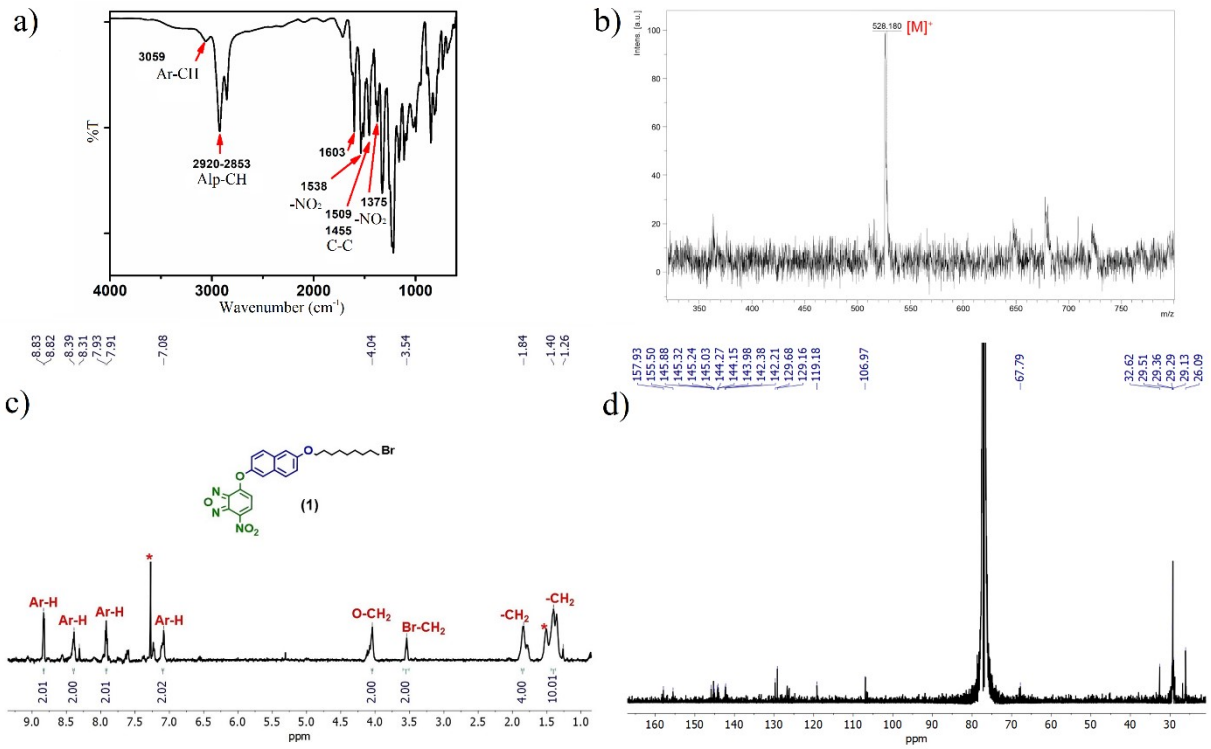

Figure S2. The structural characterization of **1**; **a)** FTIR, **b)** mass, **c)** ^{1}H NMR, and **d)** ^{13}C NMR spectra of **1**. ($CDCl_3$ was used for NMR spectra).

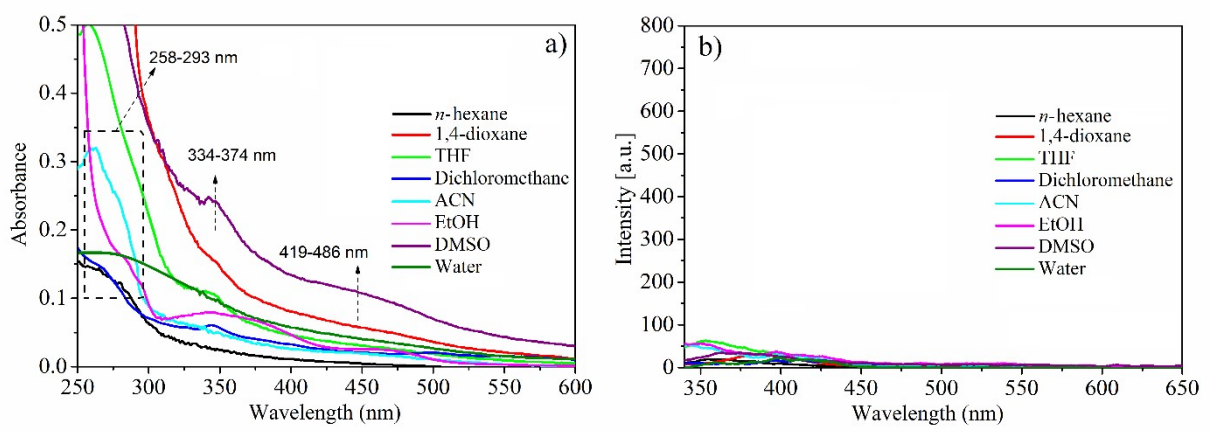

Figure S3. a) UV-Vis and **b)** fluorescence spectra of 1.00 mg.mL^{-1} ***NBD-Nap@NCC*** in different solvents.

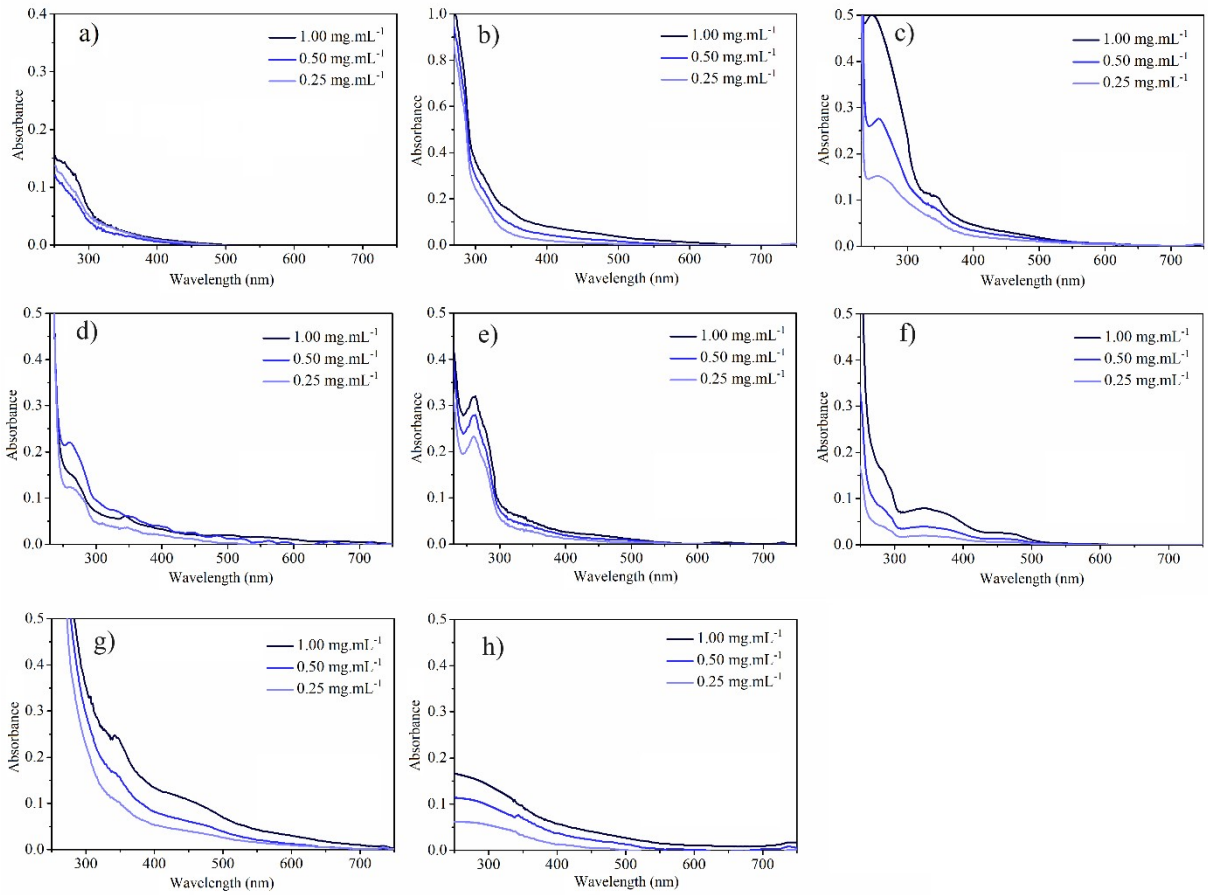

Figure S4. The UV-Vis spectra of ***NBD-Nap@NCC*** in **a)** n-hexane, **b)** 1,4-dioxane, **c)** THF, **d)** dichloromethane, **e)** ACN, **f)** EtOH, **g)** DMSO, and **h)** water at different concentrations.

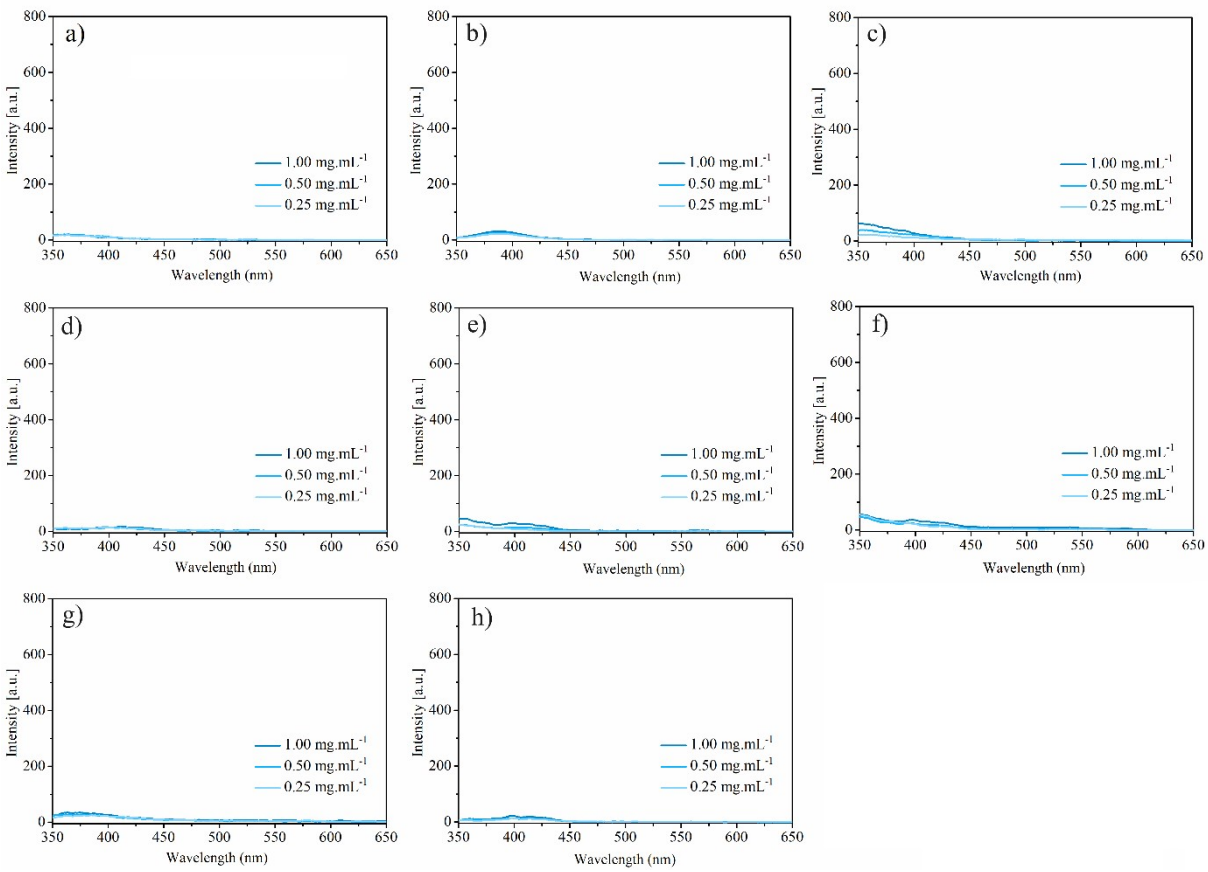

Figure S5. The fluorescence spectra of ***NBD-Nap@NCC*** in **a)** n-hexane, **b)** 1,4-dioxane, **c)** THF, **d)** dichloromethane, **e)** ACN, **f)** EtOH, **g)** DMSO, and **h)** water at different concentrations.

Table S1. The photophysical properties of ***NBD-Nap@NCC***

ε (L.g^{-1}.cm^{-1}) x10^3										
n-hexane	**1,4-dioxane**	**THF**	**Dichloromethane**	**ACN**	**EtOH**	**DMSO**	**water**	**λ_{abs} (nm)***	**λ_{ems} (nm)**	**Φ_F**
22	73	68	45	27.5	56	67	23	282, 341,465	-	<0.01

*given for wáter:EtOH

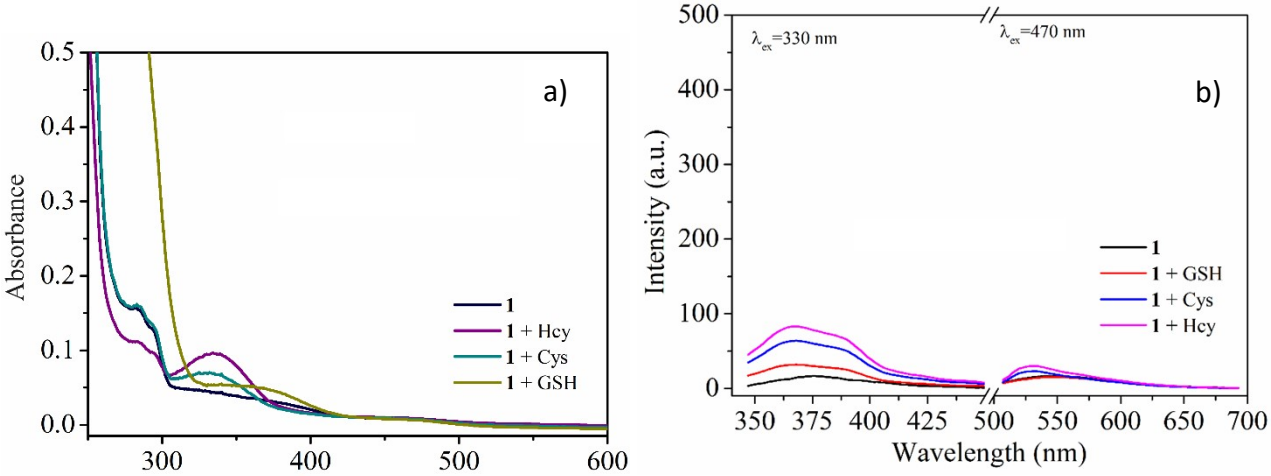

Figure S6. a) UV-Vis and **b)** fluorescence responses of **1** after addition with biothiols.

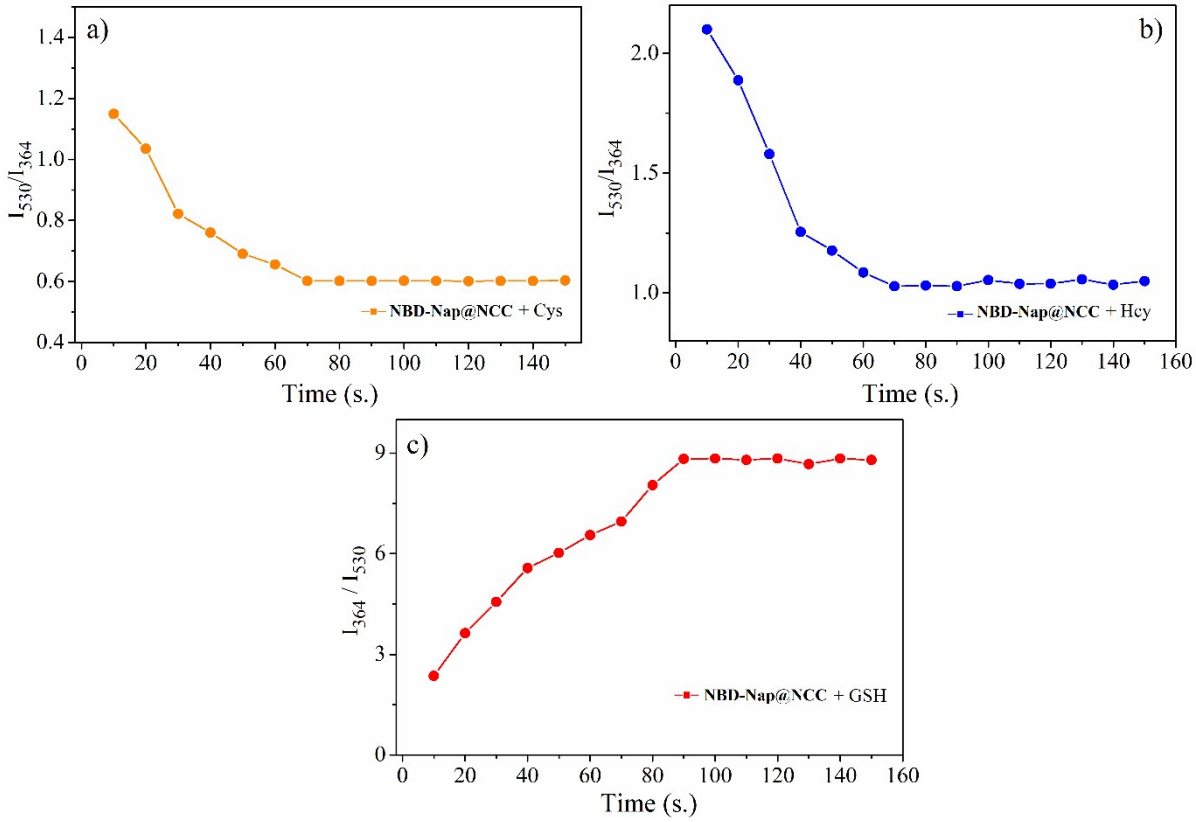

Figure S7. The optimization of interaction time of ***NBD-Nap@NCC*** with **a)** Cys, **b)** Hcy, and **c)** GSH (***NBD-Nap@NCC*****:** 1.00 mg.mL^{-1}; pH:7.0; Biothiols: 45.0 μM; in water:EtOH).

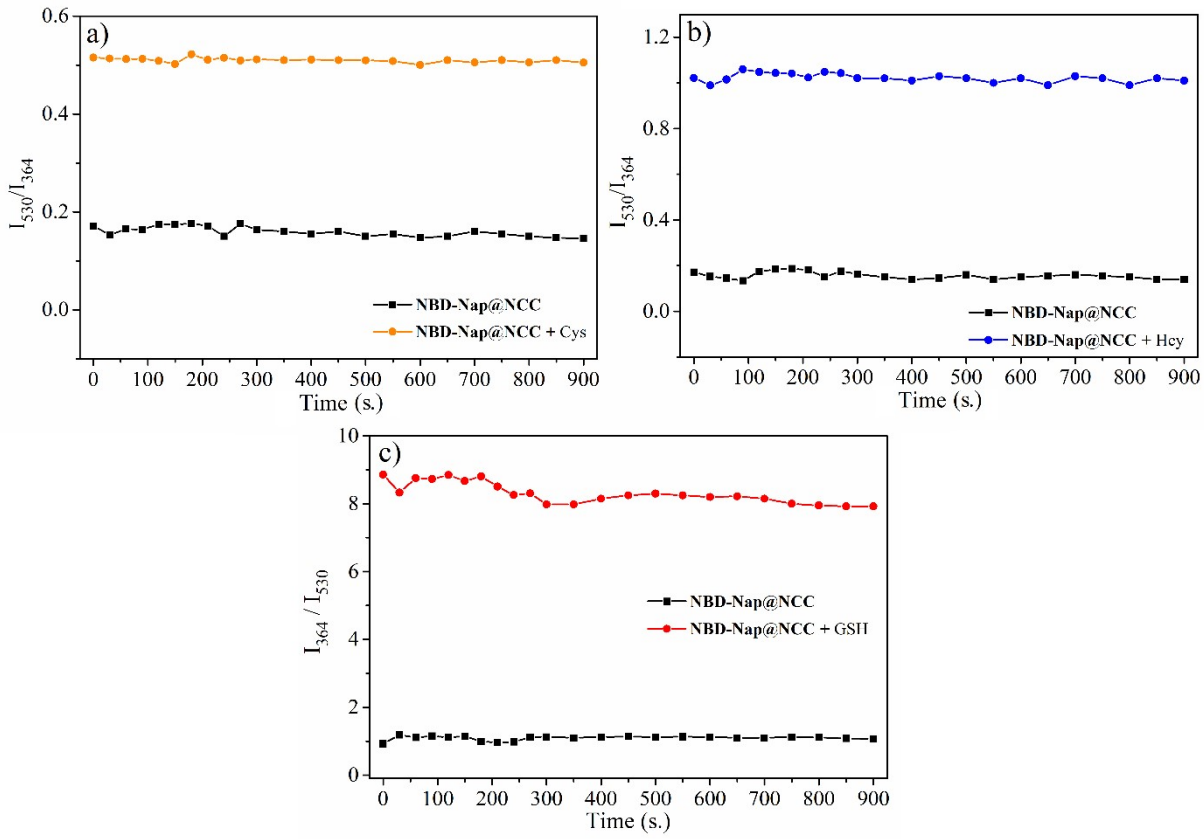

Figure S8. The photostability of ***NBD-Nap@NCC*** in presence of **a)** Cys, **b)** Hcy, and **c)** GSH (***NBD-Nap@NCC*****:** 1.00 mg.mL^{-1}; pH:7.0; Biothiols: 45.0 μM; in water:EtOH).

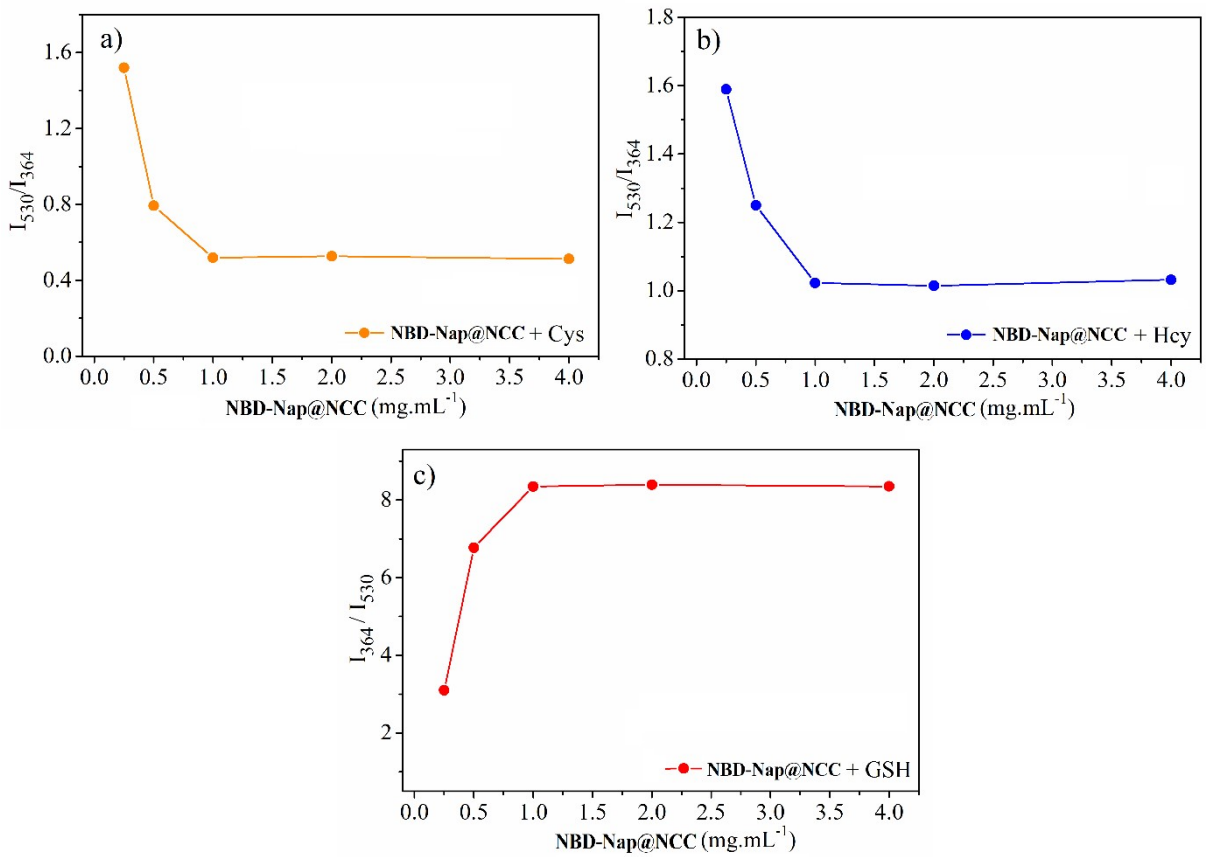

Figure S9. The optimization of initial concentration of ***NBD-Nap@NCC*** for detection of **a)** Cys, **b)** Hcy, and **c)** GSH (pH:7.0; Biothiols: 45.0 μM; in water:EtOH).

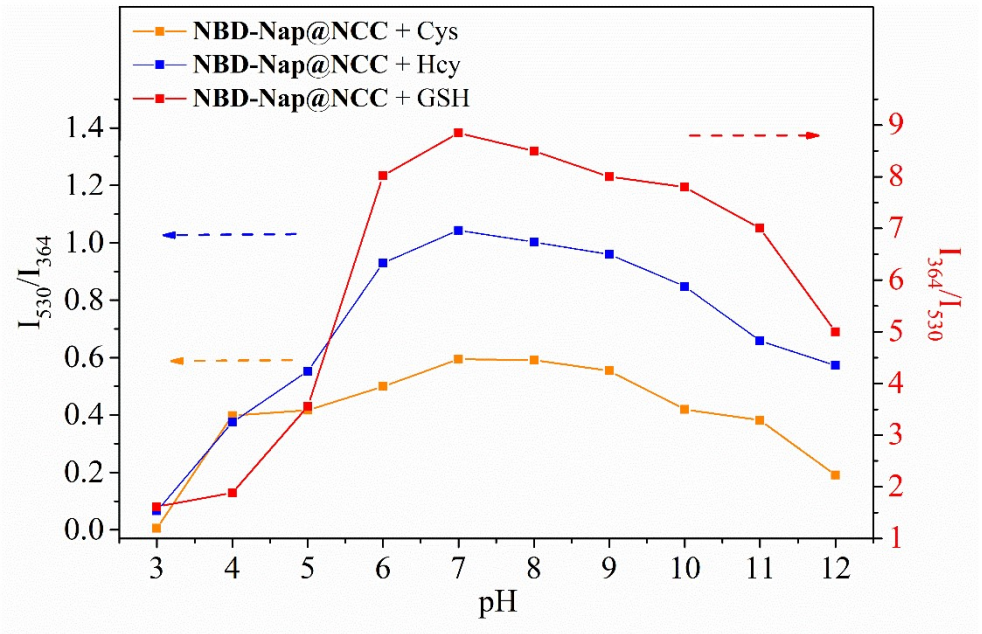

Figure S10. The optimization of pH value of sensing medium for **a)** Cys, **b)** Hcy, and **c)** GSH (***NBD-Nap@NCC*****:** 1.00 mg.mL^{-1}; Biothiols: 45.0 μM; in water:EtOH).

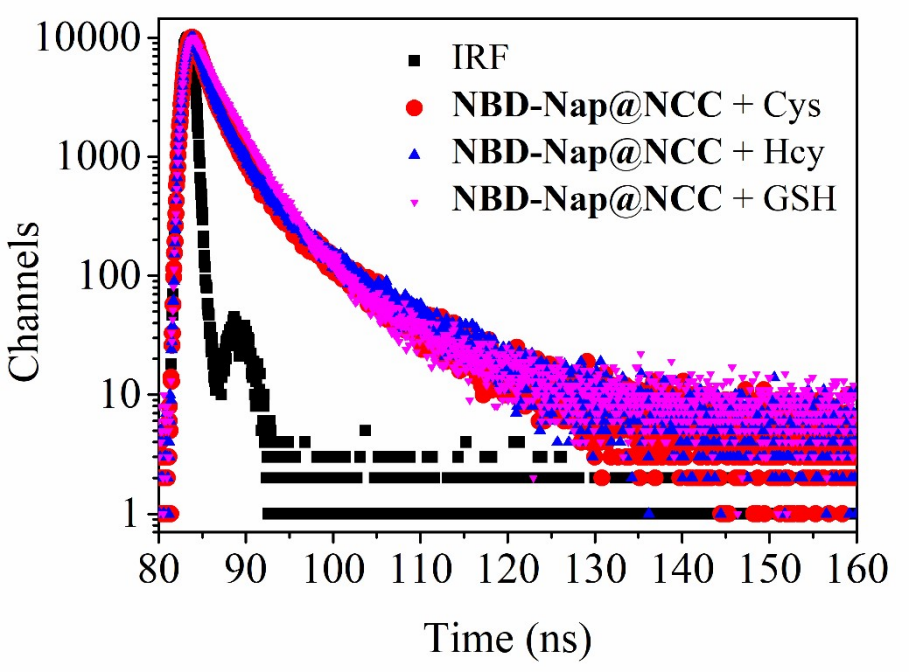

Figure S11. The time resolved fluorescence measurements for ***NBD-Nap@NCC*** in presence and absence of biothiols.

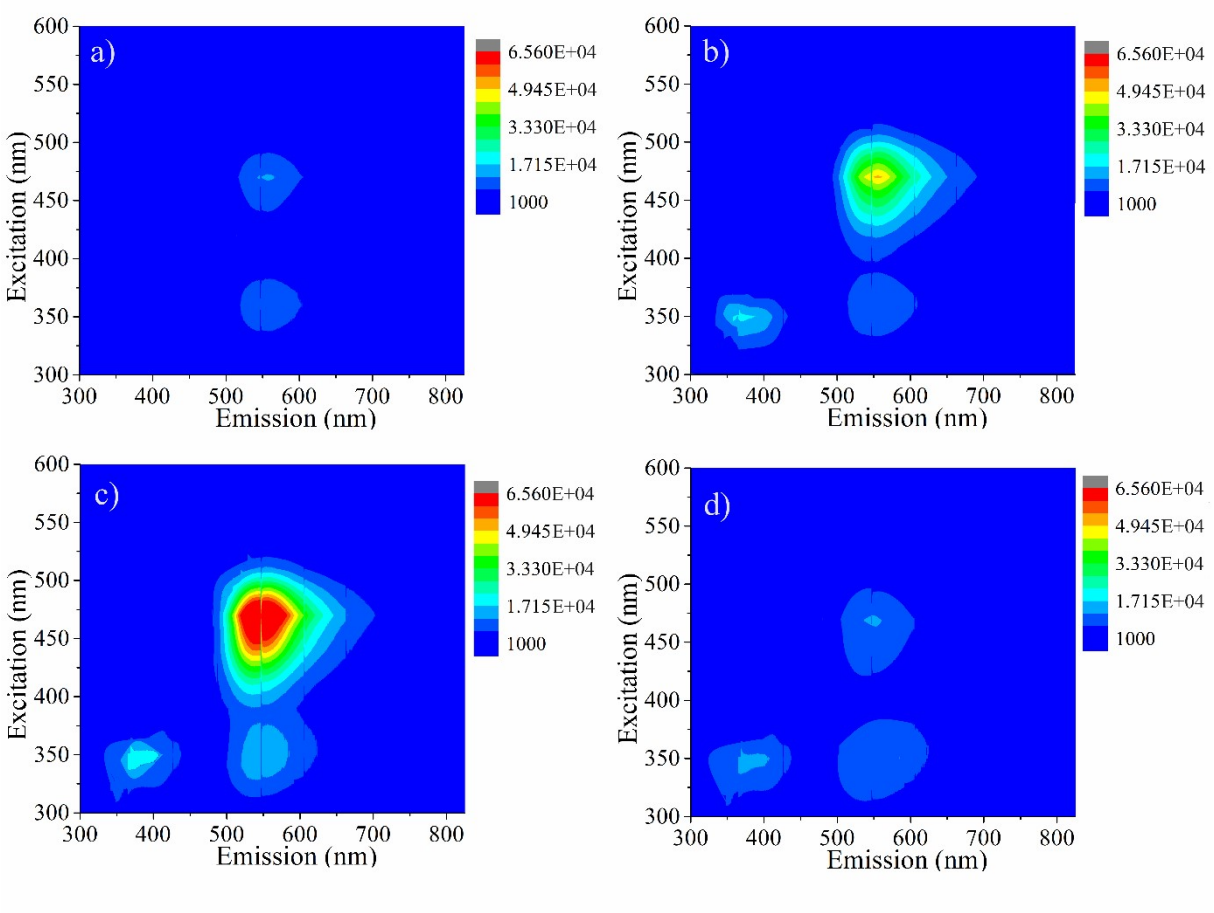

Figure S12. The EEM analyses of **a)** ***NBD-Nap@NCC***, **b)** ***NBD-Nap@NCC*** + Cys, **c)** ***NBD-Nap@NCC*** + Hcy, **d)** ***NBD-Nap@NCC*** + GSH in water:EtOH.

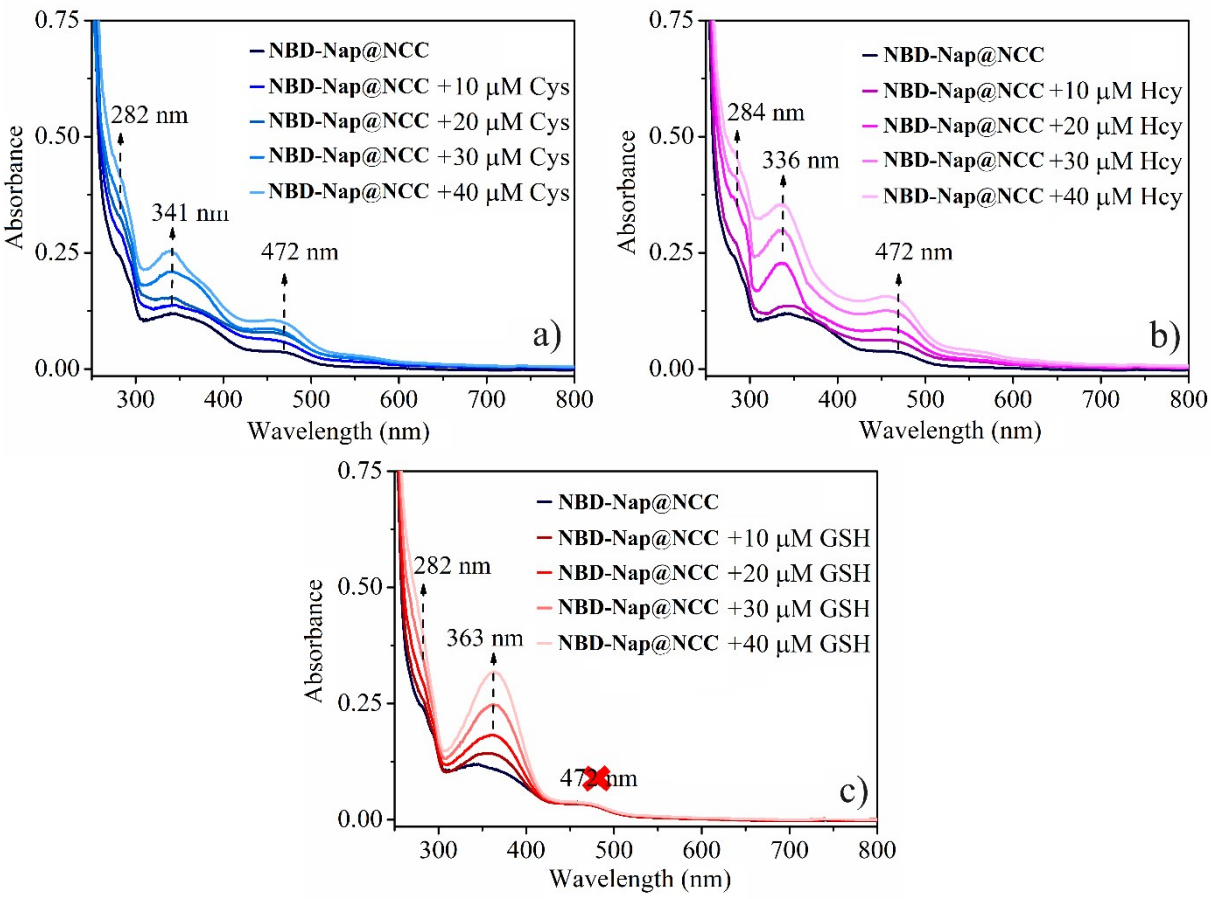

Figure S13. The UV-Vis response changes of 1.00 mg.mL^{-1} ***NBD-Nap@NCC*** after gradually increased quantity of **a)** Cys, **b)** Hcy, and **c)** GSH in water:EtOH.

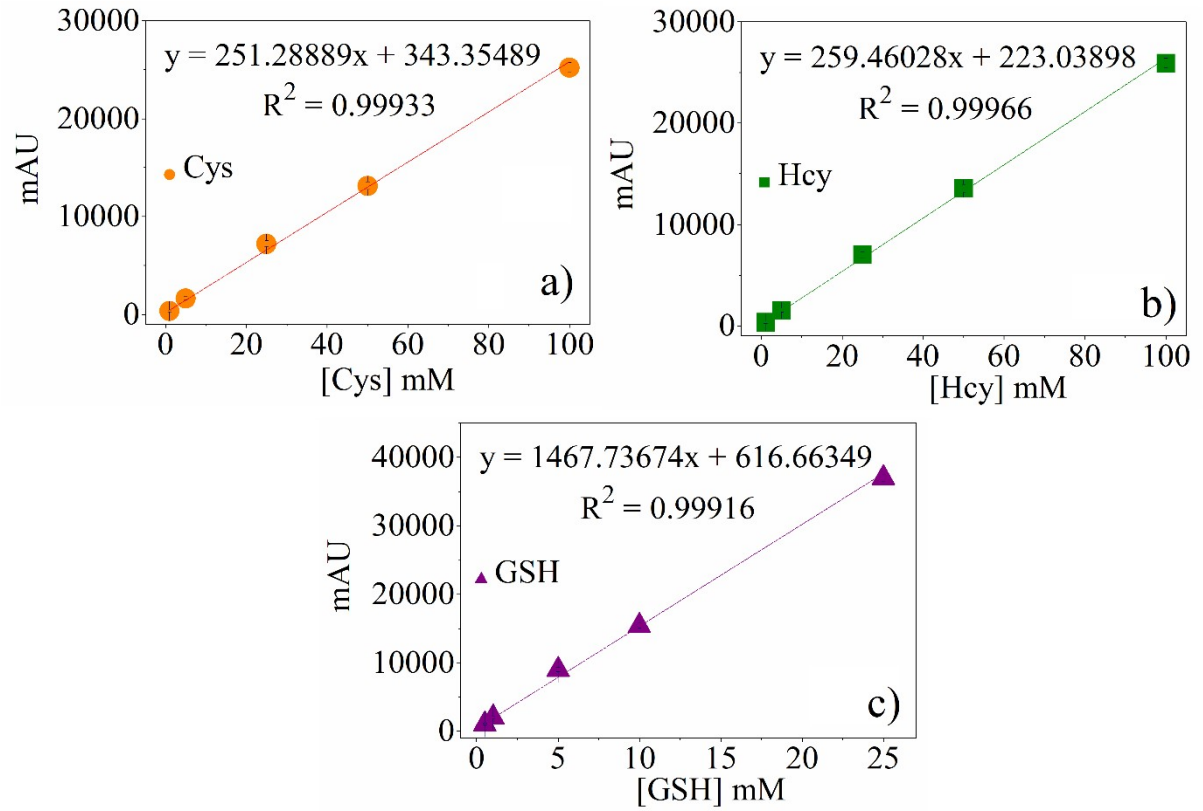

Figure S14. The calibration curves of **a)** Cys, **b)** Hcy, and **c)** GSH obtained by HPLC analysis.

Table S2. The determined analytical figures of merits for detection of biothiols with ***NBD-Nap@NCC***

Parameter	***NBD-Nap@NCC***
λ_{ex} (nm)	330/470
λ_{em} (nm)	364/530
LOD (µM)	1.150[a], 0.910[b], 1.100[c]
LOQ (µM)	3.450[a], 2.730[b], 3.320[c]
Linear range (µM)	3.50-45.00
pH	7.0
Sensor Concentration (mg.mL^{-1})	1.00
Final Volume (mL)	5.00
Medium	water:ethanol
Interaction Time (s.)	70[a], 70[b], 90[c]
R^2	0.9926[a], 0.9915[b], 0.9903[c]
RSD%	3.18[a], 3.05[b], 2.17[c]

a, b, c given for Cys; Hcy and GSH, respectively.

Table S3. The student's t-test of developed determination method based on ***NBD-Nap@NCC*** and HPLC results.

	s	X_R	$\overline{X}$	$t_{exp.}=\frac{\lvert X_R-\overline{X}\rvert}{s/\sqrt{N}}$	$t_{ref.}$	Results
Cys	4.10	165.96	160.40	2.48	4.3	2.35<4.3

Table S4. Comparison of various sensing system with ***NBD-Nap@NCC***

System	Linear Range (μM)	LOD (μM)	Interferences	Application	Ref.
GQD/AuNPs	50.0-500.0	5.88[a]	-	Urine and milk samples	[1]
GO-MnO_2	10–2000	1.53[c]	-	Live Cell imaging	[2]
Dinitrobenzenesulfonyl-derivative	0-50.0	1.47[a], 2.40[b], 2.27[c]	S^{2-}	Live Cell imaging	[3]
Benzothiazole-NBD	50.00-400.0[a] 70.00-500.0[b] 200.0-550.0[c]	4.25[a], 5.11[b], 4.30[c]	H_2S	Live Cell imaging	[4]
QD-NBD	0.50-15.00[a] 0.50-10.00[b] 0.50-12.50[c]	0.24[a], 0.21[b], 0.11[c]	NaSH	Live Cell imaging	[5]
Coumarin -NBD	20.00-100.0	0.063[a], 0.055[b], 0.057[c]	H_2S	Live Cell imaging	[6]
NBD-Nap@NCC	3.50-45.00	1.150[a], 0.910[b], 1.100[c]	-	Human serum and test kits	**This work**

References

1. C. Chaicham, T. Tuntulani, V. Promarak and B. Tomapatanaget, *Sensors and Actuators B: Chemical*, 2019, **282**, 936-944.
2. Y. Guo, X. Zhang and F.-G. Wu, *Journal of Colloid and Interface Science*, 2018, **530**, 511-520.
3. L. Qiao, Y. Yang, Y. Li, X. Lv and J. Hao, *Journal of Photochemistry and Photobiology A: Chemistry*, 2022, **425**, 113654.
4. L. He, X. Yang, K. Xu, X. Kong and W. Lin, *Chemical Science*, 2017, **8**, 6257-6265.
5. J. Zhang, H. Jia, W. Liu, J. Wang and D. Fang, *Dyes and Pigments*, 2021, **193**, 109554.
6. F. Qi, Y. Zhang, B. Wang, W. Chen, L. Yang, Z. Yang and X. Song, *Sensors and Actuators B: Chemical*, 2019, **296**, 126533.